Analytical Model of Crack Width in Hogging Moment Regions of Steel–Concrete Composite Beams Under Fatigue Loading

Aiming Song[1], Hongtao Xu[2]*, Shui Wan[3]* and Qi Luo[4]

[1]School of Civil Engineering, Yancheng Institute of Technology, Yancheng, China, [2]School of Civil Engineering, Hebei University of Science and Technology, Shijiazhuang, China, [3]School of Transportation, Southeast University, Nanjing, China, [4]School of Civil Engineering, Chongqing Jiaotong University, Chongqing, China

A modified formula for average crack spacing and a numerical model for crack width in hogging moment regions of steel–concrete composite beams under fatigue loading are proposed in this article. First, the existing calculation formulas and test data of average crack spacing are discussed and summarized. By introducing the factor of transverse reinforcement spacing, a modified formula of crack spacing is suggested based on the method of non-linear fitting. Then, a numerical model for crack width in negative moment regions under fatigue loading is proposed. In the analytical model, the explicit formulations of slip occurring at both the beam–slab interface and the reinforcement–concrete interface are included by considering fatigue effects, as well as the stress of reinforcement in the cracked section. Finally, a fatigue test on two steel–concrete composite plate beams subjected to hogging moment is designed and conducted. Compared with the crack width evaluation methods in the existing literature, the analysis results of the numerical model show more reasonable agreement with the data of the experimental beams performed in this study.

Keywords: steel–concrete composite beam, hogging moment region, fatigue, crack width, numerical model

INTRODUCTION

A steel–concrete composite beam is a new type of structure developed on the basis of steel structures and reinforced concrete structures. It has been widely accepted by the engineering field, such as buildings and bridges (Liu et al., 2016; Wang et al., 2021). The steel beam and concrete slab are combined as a whole by welding shear connectors to achieve the purpose of synergistic work. Through reasonable section design, steel–concrete composite beams can give full play to the advantages of tensile strength of steel and the compressive strength of concrete. However, in the negative moment regions near the intermediate support of steel–concrete continuous composite beams, a complex non-linear behavior under the action of a low static load is due to the existence of adverse factors such as concrete tension and steel beam compression (Chen et al., 2009; Sun et al., 2014). In addition, under the long-term action of fatigue loads such as moving vehicles and wind strength, the service performance and durability of the structure are often further weakened (Wang et al., 2018). Among these shortcomings, cracking of the concrete slab has been one of the most crucial issues in hogging moment regions in composite girder bridges. For the design of a steel–concrete composite bridge, it is an economical and convenient solution to allow for the

formation of cracks within the limit of acceptable widths (Ryu et al., 2004; Ryu et al., 2007). Moreover, the introduction of high-performance materials such as engineered cementitious composites (ECCs) (Qin et al., 2020; Zhang et al., 2021; Zhang et al., 2022) and ultra-high performance concrete (UHPC) (Luo et al., 2020) also provides an effective method for crack control.

There have been considerable experimental and theoretical studies on the concrete cracking and crack control of composite beams subjected to negative moments in the past. Ryu et al. (2007) studied the crack development and crack control measures in negative bending moment regions through fatigue loading tests of a full-size model of a two-span continuous composite beam manufactured with a prefabricated concrete slab. The structural strength and stiffness under fatigue loading still presented a good performance for the composite section, and the crack width of the prefabricated slab can be effectively controlled within the allowable range. El-Shihy et al. (2010) and El-Zohairy et al. (2017) conducted experimental tests and finite element analysis on composite beams under negative moments bonded with CFRP laminates. The results showed that CFRP laminates can effectively improve the cracking performance and bearing capacity in negative bending moment regions. Su et al. (2012) conducted an experimental study on the inelastic behavior in negative moment regions of steel–concrete composite box girders manufactured with inclined webs. The results showed that the longitudinal reinforcement ratio has an important influence on the crack propagation of concrete slabs, and the higher the reinforcement ratio, the better the effect of crack control. Fan et al. (2020) conducted static loading tests on steel and ECC beams under negative moment by taking the reinforcement ratio as the characteristic parameter. The results showed that ECC could significantly improve the stiffness and crack resistance of composite beams in the negative moment regions. Based on the four-parameter fiber bridge model, the tensile hardening equation of reinforced ECC members was deduced, and the crack width in negative moment regions of steel–ECC beams was calculated and analyzed. Song et al. (2021) developed a numerical calculation model of the crack width of steel–concrete composite beams under static negative moment regions by taking the bond–slip relationship at the reinforcement–concrete interface and the slip effect at the beam–slab interface into consideration. In addition, it was reported that the development of cracks is decisively influenced by transverse reinforcement (Ryu et al., 2005; He et al., 2010). To determine the minimum reinforcement with reference to the service load and to calculate the crack width, the transverse reinforcement must be taken into account (Ramm and Elz, 2002).

Till now, there are still no standard and applicable analytical methods for crack spacing and crack width in the negative moment regions of steel–concrete composite beams in the present design codes. In Eurocode 4-2 (2005), a simple way is suggested that crack width under negative moment could be calculated according to Eurocode 2 (2004). In China Code GB 50917-2013 (2013), the calculation formula for crack width in China Code GB 50010-2010 (2010) is employed to check the crack width of continuous composite beams. Moreover, very limited reports have studied the development laws of crack spacing and crack width in negative moment regions. Nie and Zhang (1997) conducted an experimental study on four simply supported composite steel–concrete beams under negative moments and two continuous two-span composite beams under point loads. Based on the experimental results and analysis, the formulas were proposed for estimating crack spacing and maximum crack width, which have been applied to the design practice of engineering. Yu and Guo (2004) conducted an experiment of eighteen partially prestressed steel-concrete composite beams subjected to negative moment. In terms of the test results, the formulas for calculating crack width in the negative bending region were presented, which coincided well with the current code for the design of concrete structures.

However, it is found that the models of present codes proposed to calculate the crack width of composite beams were employed from axial tension members, while the combination effect of steel beam on concrete slab was not fully considered. Like the analytical models presented in some existing literature, the fitted data from the tests conducted previously was limited and the slip at the beam–slab interface was not included. As a result, the existing models may attain unreasonable crack widths in the negative moment regions. For these reasons, it is very important to have a reliable analysis method for crack width that takes into account the effective behavior of steel–concrete composite beams under hogging moment. As a detailed and accurate method in the last decades, the finite element model based on suitable numerical procedures was utilized for the analysis of non-linear mechanical behavior and the calculation of crack width of reinforced concrete beams (Manfredi and Pecce, 1998; Fabbrocino et al., 2007; Oliveira et al., 2008; Castel et al., 2012), as well as the overall flexural behavior of composite beams under hogging moment (Manfredi et al., 1999). However, few researchers have conducted numerical research on crack width in the negative moment regions of continuous composite beams. In addition, most of the analytical methods were presented statically, while fatigue effects were rarely considered.

Set against the above background, this study aims to investigate the analytical methods of crack spacing and crack width in the hogging moment regions of steel–concrete composite beams under fatigue loading. A modified formula for crack spacing is suggested based on the existing equations by introducing the factor of transverse reinforcement spacing. The parameter associated with transverse reinforcement spacing is achieved by fitting the data from this study and some literature data. Owing to the fact that the current studies have not yet included an accurate method to evaluate the crack width in the negative moment regions of continuous composite beams considering fatigue effect, a numerical model is then proposed that includes explicit formulations of slip occurring at both the beam–slab interface and the reinforcement–concrete interface. Finally, a fatigue test on a steel–concrete composite plate beam subjected to hogging moment was conducted. Through comparing with the measured values of experimental work and the crack width evaluation methods in existing literature, the analysis results of the numerical model were verified.

MODIFIED FORMULA FOR AVERAGE CRACK SPACING

Crack spacing directly affects the crack width of concrete. When the fatigue upper limit of the test beam is set at the crack development stage, new cracks will occur after a certain number of repeated cycles. And with the increase in loading times, the number of cracks tends to be stable. However, fatigue loading has little influence on the final crack spacing in the negative moment regions of composite beams when compared with static loading, which is similar to the development law obtained in reinforced concrete structures (Song, 2006). Therefore, the calculation method of the average crack spacing given in this section can be applied to the composite beams with studs both under fatigue loading and static loading, which can provide a basis for the establishment of the analytical method of crack width in the negative moment regions in the following section.

Analysis of Existing Formula for Average Crack Spacing

At present, several formulas have been proposed to predict the average crack spacing in the negative moment regions of continuous composite beams. However, the views on the influence factors of the existing formulas are not yet unified. The models employed by the design codes to calculate the average crack spacing were based on reinforced concrete structures, while the factors associated with composite beams were not fully taken into account. The common models in CEB-FIP (1978), China Code GBJ 10-89 (1989) and China Code GB 50010-2010 (2010) can be expressed, respectively, as follows:

$$l_{cr} = 2\left(c_s + \frac{l_s}{10}\right) + k_1 k_2 \frac{d_{eq}}{\rho_{te}}, \tag{1}$$

$$l_{cr} = 1.1\left(2.7c_s + 0.11\frac{d_{eq}}{\rho_{te}}\right)\nu, \tag{2}$$

$$l_{cr} = 1.1\left(1.9c_s + 0.08\frac{d_{eq}}{\rho_{te}}\right). \tag{3}$$

An improved model based on China Code GBJ 10-89 (1989) was proposed by Wu et al. (1993), while the transverse reinforcement ratio and diameter were considered. The equation obtained was then as follows:

$$l_{cr} = 2.7c_s + \frac{0.1}{\rho_{te}/d_{eq} + 1.2\rho_{Hte}/d_{Heq}}. \tag{4}$$

As the aforementioned models for average crack spacing showed no relation with the combination effect, the previous studies took the combined force ratio and spacing of stud connectors into consideration (Nie and Zhang, 1997; Yu and Guo, 2004), and two novel models were then proposed according to China Code GBJ 10-89 (1989) and China Code GB 50010-2010 (2010). The two equations are shown, respectively, as follows:

$$l_{cr} = 1.1\left(2.7c_s + \frac{0.11}{\rho_{te}/d_{eq} + 0.25R_p^2/p}\right)\nu \tag{5}$$

$$l_{cr} = 1.9c_s + \frac{0.08}{\rho_{te}/d_{eq} + 0.04R_p^2/p}. \tag{6}$$

The development of cracking in slabs as part of composite beams is decisively influenced by the transverse reinforcement (Ramm and Elz, 2002). But this influence factor was not considered in the models mentioned earlier. A simple model which took the combined force ratio and transverse reinforcement spacing into account was established then by Zhang et al. (2011), while other important factors were not taken into account. The equation is given as follows:

$$l_{cr} = l_a\left(1 - R_p^3\right). \tag{7}$$

In the aforementioned equations, l_{cr} is the average crack spacing; k_1 is the bonding performance coefficient of longitudinal tensile bars, and $k_1 = 0.4$ is for a deformed bar; k_2 is the influence coefficient of component stress distribution, and $k_2 = 0.25$ is for a tension member; ν is the surface characteristics coefficient of longitudinal tensile bars, and $\nu = 0.7$ is for deformed bar; c_s is the concrete cover thickness of reinforcement; l_s and l_a are the spacings of longitudinal reinforcement and transverse reinforcement, respectively; d_{eq} and d_{Heq} are the equivalent diameters of longitudinal tensile bars and transverse bars, respectively; ρ_{eq} and ρ_{Heq} are the tensile reinforcement ratio and transverse reinforcement ratio, respectively; R_p is the combined force ratio; and p is the spacing of stud connectors.

In summary, the average crack spacing in the negative moment regions of continuous composite beams is mainly related to the concrete cover thickness of reinforcement, equivalent diameters of longitudinal tensile bars, the tensile reinforcement ratio, the combined force ratio, the spacing of stud connectors, and transverse reinforcement. However, the influence factors considered in the existing formulas mentioned before, proposed by researchers and codes, were not comprehensive.

Analysis of a Modified Formula for Average Crack Spacing

In this section, a total of 38 specimen tests from previous literature were summarized and analyzed to study the influence factors of average crack spacing, as can be seen in **Table 1**. According to **Eq. 6**, which was based on China Code GB 50010-2010 (2010), a modified formula of crack spacing was proposed by introducing the factor of transverse reinforcement spacing l_a and taking the consistency of dimension into consideration. The parameters were achieved by fitting the data listed in **Table 1** with the procedure shown in **Figure 1**. In this way, the novel model obtained was then as follows:

$$l_{cr} = 1.9c_s + \frac{0.08}{0.25\rho_{te}/d_{eq} + 0.05R_p^2/p + 0.07/l_a}. \tag{8}$$

TABLE 1 | Analysis of experimental test data obtained from the existing literature.

Specimen		Test results l_{cr} (mm)	Equation 3 l_{cr3} (mm)	l_{cr}/l_{cr3}	Equation 4 l_{cr4} (mm)	l_{cr}/l_{cr4}	Equation 5 l_{cr5} (mm)	l_{cr}/l_{cr5}	Equation 6 l_{cr6} (mm)	l_{cr}/l_{cr6}	Equation 7 l_{cr7} (mm)	l_{cr}/l_{cr7}	Equation 8 l_{cr8} (mm)	l_{cr}/l_{cr8}
Nie and Zhang (1997)	SCB1	188	109.3	1.72	105.8	1.77	112.3	1.67	108.5	1.73	198.6	0.94	165.0	1.14
	SCB2	169	97.3	1.74	100.4	1.69	90.9	1.86	94.8	1.78	185.2	0.91	147.0	1.15
	SCB3	207	109.3	1.89	105.8	1.95	112.3	1.84	108.5	1.90	198.6	1.04	161.9	1.28
	SCB4	214	109.3	1.96	105.8	2.02	108.1	1.98	107.8	1.99	198.6	1.08	162.0	1.32
	SCB5	167	97.3	1.71	100.4	1.66	82.2	2.03	92.5	1.80	185.2	0.90	133.9	1.25
	SCB6	200	109.3	1.83	105.8	1.89	108.1	1.85	107.8	1.86	198.6	1.01	159.1	1.26
Ryu et al. (2005)	CR1	165	145.0	1.14	—	—	154.5	1.07	144.8	1.14	172.2	0.96	183.2	0.90
Yu and Guo (2004)	SCB-1	121	130.9	0.92	108.0	1.12	85.7	1.41	113.8	1.06	77.3	1.57	111.5	1.09
	SCB-2	129	130.9	0.99	108.0	1.19	91.9	1.40	117.4	1.10	77.3	1.67	115.7	1.11
	SCB-3	125	130.9	0.95	108.0	1.16	96.8	1.29	119.7	1.04	77.3	1.62	118.6	1.05
	SCB-4	146	209.2	0.70	104.4	1.40	127.6	1.14	182.0	0.80	87.5	1.67	131.8	1.11
	SCB-5	123	136.9	0.90	99.6	1.23	98.4	1.25	124.1	0.99	77.3	1.59	119.6	1.03
	SCB-6	135	183.1	0.74	103.1	1.31	86.1	1.57	137.1	0.98	34.1	3.95	112.8	1.20
	SCB-7	119	163.3	0.73	101.9	1.17	70.7	1.68	108.8	1.09	90.7	1.31	96.2	1.24
	SCB-8	95	98.9	0.96	94.0	1.01	78.5	1.21	91.5	1.04	46.9	2.03	103.9	0.91
	CCB-1	115	130.9	0.88	108.0	1.06	94.9	1.21	118.8	0.97	81.5	1.41	117.5	0.98
	CCB-2	110	134.2	0.82	108.6	1.01	99.0	1.11	122.7	0.90	85.1	1.29	119.8	0.92
	CCB-3	119	195.8	0.61	116.3	1.02	96.5	1.23	153.1	0.78	71.3	1.67	119.8	0.99
	CCB-4	140	272.7	0.51	121.2	1.16	173.7	0.81	242.8	0.58	96.4	1.45	140.9	0.99
	CCB-5	85	130.9	0.65	108.0	0.79	77.9	1.09	107.7	0.79	36.4	2.34	104.6	0.81
	CCB-6	141	209.2	0.67	104.4	1.35	142.5	0.99	189.0	0.75	92.6	1.52	135.2	1.04
	CCB-7	130	136.9	0.95	99.6	1.30	101.6	1.28	125.5	1.04	81.5	1.60	121.1	1.07
	CCB-8	89	105.4	0.84	95.3	0.93	73.2	1.22	92.0	0.97	—	—	98.6	0.90
	CCB-9	128	136.9	0.94	99.6	1.28	109.4	1.17	128.5	1.00	81.5	1.57	124.4	1.03
	CCB-10	122	136.9	0.89	99.6	1.22	96.3	1.27	123.1	0.99	81.5	1.50	118.5	1.03
Hou et al. (2001)	T1	89	96.6	0.92	115.9	0.77	103.7	0.86	96.5	0.92	139.2	0.64	136.2	0.65
	T2	89	96.6	0.92	115.9	0.77	102.9	0.87	96.4	0.92	139.2	0.64	135.5	0.66
Zhang et al. (2011)	CCB-1	112	143.5	0.78	116.5	0.96	141.3	0.79	141.4	0.79	74.1	1.51	116.2	0.96
	CCB-2	72	95.3	0.76	102.2	0.70	86.2	0.84	91.9	0.78	63.8	1.13	100.4	0.72
	SCB-5	145	143.5	1.01	116.5	1.24	146.1	0.99	142.3	1.02	74.1	1.96	116.8	1.24
	SCB-6	103	119.7	0.86	110.7	0.93	119.1	0.86	118.1	0.87	71.8	1.43	112.0	0.92
	SCB-7	81	109.4	0.74	107.5	0.75	105.7	0.77	107.3	0.75	69.8	1.16	108.4	0.75
	SCB-8	78	95.3	0.82	102.2	0.76	91.4	0.85	93.2	0.84	63.8	1.22	102.8	0.76
Wu et al. (1993)	L-1	123	160.0	0.77	116.3	1.06	158.1	0.78	157.8	0.78	148.4	0.83	170.8	0.72
	L-2	108	122.8	0.88	110.1	0.98	112.4	0.96	119.1	0.91	138.9	0.78	148.4	0.73
	L-3	116	122.8	0.94	116.4	1.00	112.6	1.03	119.1	0.97	185.2	0.63	164.7	0.70
	L-4-L	89	94.1	0.95	104.0	0.86	83.7	1.06	90.0	0.99	114.3	0.78	118.2	0.75
	L-4-R	100	94.1	1.06	107.5	0.93	83.7	1.20	90.0	1.11	152.3	0.66	125.0	0.80
Statistical results	Average value			1.001		1.174		1.223		1.072		1.350		0.978
	Standard deviation			0.377		0.349		0.359		0.361		0.608		0.193
	Coefficient of variation			0.377		0.297		0.293		0.337		0.450		0.198

The physical meaning of **Eq. 8** is consistent with **Eqs. 1–7** which were empirical formulas derived from data fitting. To verify the validity of the modified model described before, existing experiments conducted by Song et al. (2021) and He et al. (2010) were selected and analyzed with other proposed models expressed in **Eqs 3–7**. As is shown in **Table 2**, the maximum error was controlled within 10% for **Eq. 8**. Generally, it can be seen that the results of the modified formula are in better agreement with the experimental results compared with existing models. Hence, it is effective to use the modified model to study the average crack spacing in the negative moment regions of continuous composite beams.

ANALYTICAL MODEL FOR CRACK WIDTH UNDER FATIGUE LOADING

Crack opening of reinforced concrete beams under fatigue loading depends on several factors, most of which can be related to bond quality and to the effective area where reinforcement–concrete bond interaction may develop (Fabbrocino et al., 2007). As for composite beams, shear force at the beam–slab interface should also be included as an important factor in the analysis of the cracked section (Manfredi et al., 1999). In order to model these behaviors, it is

FIGURE 1 | Flowchart of the fitting procedure.
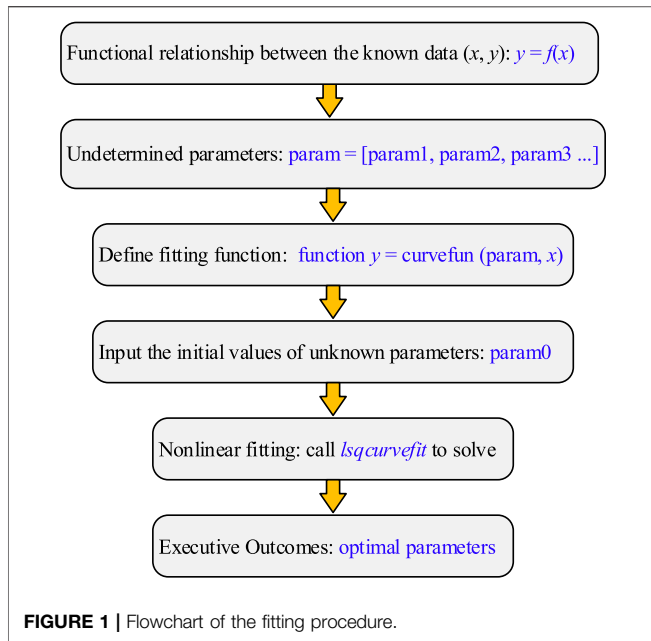
necessary to give suitable constitutive laws of materials and an analytical model for crack width prediction.

Constitutive Relations
Material Models
When the fatigue upper limit is reached under normal service conditions, cracks in the concrete slab of composite beams under hogging moment will develop into the stabilized stage after a certain number of repeated cycles, and crack spacing will be almost unchanged. Then it can be assumed that the material properties between the two cracks in the negative moment regions of continuous composite beams under fatigue loading can be considered linear elastic (Han et al., 2014). Thus, the stress–strain laws considering the fatigue effect of steel and concrete in tension can be formally expressed as follows:

$$\begin{cases} \sigma_{ct}(n) = E_c \varepsilon_{ct}(n) \\ \sigma_s(n) = E_s \varepsilon_s(n) \end{cases}, \tag{9}$$

where $\sigma_{ct}(n)$ and $\sigma_s(n)$ are stresses of concrete and steel under fatigue loading; $\varepsilon_{ct}(n)$ and $\varepsilon_s(n)$ are strains of concrete and steel under fatigue loading; and E_c and E_s are the young's modulus of concrete and steel, respectively.

Bond Behavior of Reinforcing Bars
Slip at the reinforcement–concrete interface kept increasing, due to the gradual deterioration of the bond property between these two materials. When the limit of bonding stress is kept constant during the fatigue loading process, the total slip increases with the repeated cycles characterized as an S-shaped curve (Balázs, 1991), as exhibited in **Figure 2A**. When the slip develops to stage III, as shown in **Figure 2A**, the reinforced concrete member is close to the state of pull-out failure. This stage is generally not considered in the theoretical analysis. Then the growth trend of slip at stage I and stage II can be approximated in exponential form (Zanuy et al., 2010). Therefore, the bond–slip relationship between reinforcement and concrete caused by fatigue loading can be directly determined by peak slip under static loading s_1, and the peak slip after a certain number of loading cycles of n can be expressed as follows (Zhang et al., 2017):

$$s_1^f(n) = s_1(1+n)^{0.107}. \tag{10}$$

From the perspective of energy dissipation, the fatigue loading process of materials is the same as that of static loading (Liu and Zhou, 2018). In the reinforced concrete structure, it is shown as follows: when the bond failure occurs between the reinforcement and the concrete for a certain number of repeated cycles, the maximum slip under fatigue loading is basically consistent with the slip value on the descending section of the bond stress–slip curve under pure static loading corresponding to the maximum bond stress. Therefore, the descending section of the bond–slip curve under static loading can be used to represent the envelope curve of the remaining bonding strength under fatigue load, as shown in **Figure 2B**.

In this section, the four-linear bond–slip model between concrete and reinforcing bars suggested in CEB-FIP Model Code 1990 (1993) was employed. The following relations give its analytical formulation:

$$\begin{cases} \tau = \tau_{max} \cdot \left(\dfrac{s}{s_1}\right)^{\alpha}, & 0 \le s \le s_1 \\ \tau = \tau_{max}, & s_1 \le s \le s_2 \\ \tau = \tau_{max} - (\tau_{max} - \tau_f) \cdot \left(\dfrac{s - s_2}{s_3 - s_2}\right), & s_2 \le s \le s_3 \\ \tau = \tau_f, & s \ge s_3, \end{cases} \tag{11}$$

where τ_{max} is the ultimate bonding strength, $\tau_{max} = 2.0\sqrt{f_c'}$; f_c' is the compressive strength of concrete cylinders; $\tau_f = 0.15\tau_{max}$; $\alpha = 0.4$; $s_1 = 0.6$; and $s_2 = 0.6$; $s_3 = 1$.

TABLE 2 | Comparison of experimental and modeling results.

| Specimen		Test results l_{cr} (mm)	Equation 3		Equation 4		Equation 5		Equation 6		Equation 7		Equation 8	
			l_{cr3} (mm)	l_{cr}/l_{cr3}	l_{cr4} (mm)	l_{cr}/l_{cr4}	l_{cr5} (mm)	l_{cr}/l_{cr5}	l_{cr6} (mm)	l_{cr}/l_{cr6}	l_{cr7} (mm)	l_{cr}/l_{cr7}	l_{cr8} (mm)	l_{cr}/l_{cr8}
Song et al. (2021)	SCB1-1	105	92.6	1.13	112.9	0.93	93.5	1.12	91.4	1.15	87.6	1.20	115.9	0.91
He et al. (2010)	CB-1-1	95	63.3	1.50	63.6	1.49	65.6	1.45	62.9	1.51	87.0	1.09	86.8	1.09
	CB-1-2	94	63.3	1.48	63.6	1.48	65.6	1.43	62.9	1.49	87.0	1.08	86.8	1.08
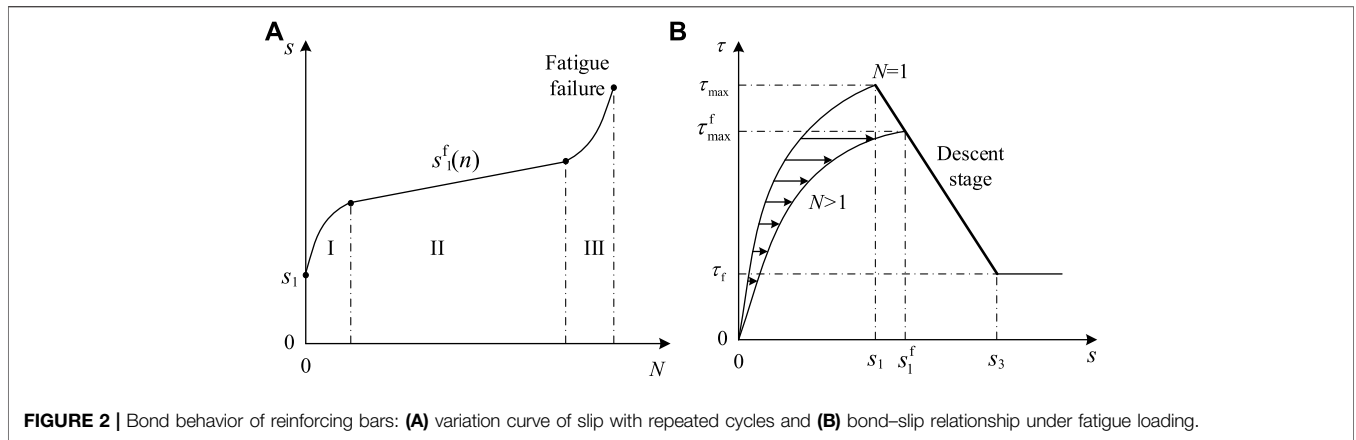
FIGURE 2 | Bond behavior of reinforcing bars: **(A)** variation curve of slip with repeated cycles and **(B)** bond–slip relationship under fatigue loading.

Then the maximum bonding stress τ_{max}^f after repeated cycles of n can be calculated according to peak slip $s_1^f(n)$, as follows:

$$\tau_{max}^f = \tau_{max} - (\tau_{max} - \tau_f) \cdot \left(\frac{s_1^f(n) - s_1}{s_3 - s_1} \right) \qquad (12)$$

Shear at the Beam–Slab Interface

At present, the degradation of strength or stiffness of stud connectors in steel–concrete composite structures under fatigue loading has been studied (Hanswille et al., 2007a). According to the experimental study in the literature (Hanswille et al., 2007b), the deformation behavior of stud connectors under fatigue loading is mainly characterized by increasing residual slip and elastic shear stiffness. The load–slip (P_n–δ_n) curve after n loading cycles can be expressed by the residual shear capacity $P_{u,n}$, in the following form:

$$P_n = K_{el,n} \cdot P_{u,n} \cdot (\delta_n - \delta_{std,N}), P_n \leq 0.8 P_{u,n}. \qquad (13)$$

The residual slip $\delta_{std,N}$ between the stud and concrete after fatigue loading can be expressed as follows (Hanswille et al., 2007a):

$$\delta_{std,N} = C_1 - C_2 \ln \left(\frac{1}{n/N_f} - 1 \right) \geq 0, \quad 0 < n \big/ N_f < 0.9 \qquad (14)$$

$$\delta_{std,N} = 0, \quad n/N_f = 0, \qquad (15)$$

where the coefficients C_1 and C_2 are given as follows:

$$C_1 = 0.104 e^{3.95 P_{max}/P_{u,0}} \qquad (16)$$

$$C_2 = 0.664 P_{min} \big/ P_{u,0} + 0.029. \qquad (17)$$

Then the interface shear–slip (v_n–δ_n) relationship at the beam–slab interface under fatigue loading can be given as follows:

$$v_n = \frac{K_n \cdot \delta_n}{p}. \qquad (18)$$

After n loading cycles, the residual stiffness $K_{s,n}$ of the stud connectors can be expressed as follows:

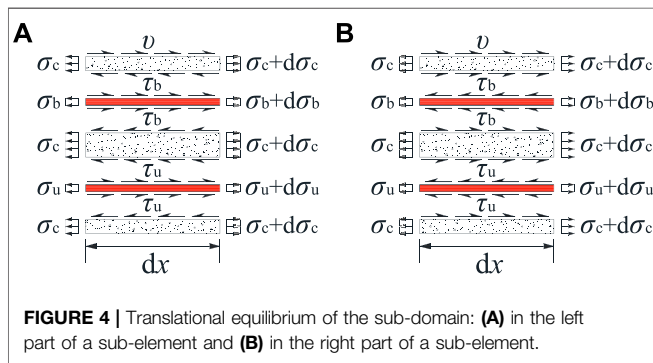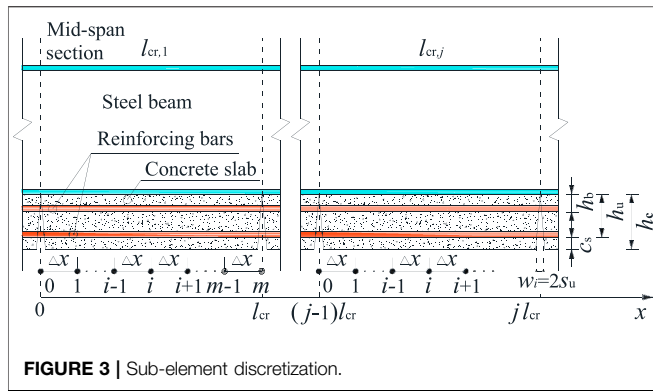$$K_{s,n} = K_{el,n} \cdot P_{u,n}. \qquad (19)$$

The residual shear capacity $P_{u,n}$ can be determined by the following formula:

$$\frac{P_{u,n}}{P_{u,0}} = 0.74 \frac{P_{max}}{P_{u,0}} \left(1 - \frac{\Delta P}{P_{max}} \right) + 0.54$$

$$- 0.04 \ln \left(\frac{n}{10^{0.1267 - 0.1344 \frac{P_{max}}{P_{u,0}} \left(1 - \frac{\Delta P}{2P_{u,0}} \right)} - n} \right). \qquad (20)$$

In the formulas given earlier, n denotes the number of repeated cycles; N_f is the fatigue life of studs; $K_{el,n}$ is a constant, and it is equivalent to 1.41 (unit: mm^{-1}); $K_n = n_s K_{s,n}$; p is the longitudinal spacing of the studs; $P_{u,0}$ and ΔP are the ultimate static strength and shear amplitude of the studs, respectively; $\Delta P = P_{max} - P_{min}$; and P_{max} and P_{min} are the fatigue upper limit and fatigue lower limit of studs, respectively.

Stress of Reinforcing Bar in Cracked Section

The fatigue stress state of the reinforcing bar in the concrete slab of composite beams under negative moment is basically the same as that of a reinforced concrete structure. With the increase of repeated cycles, the effective tensile area of the reinforcing bar will decrease, especially at the cracking location (Song, 2006). When the loss of cross-sectional area of the reinforcing bar in the process of fatigue loading conforms to Miner's rule, the effective area of reinforcing bar at cracking position after n cycles can be determined by **Eq. 21**. Considering the degradation of the effective area of the reinforcing bar and the shear stiffness of studs under fatigue loading, an equation proposed by Fan and Nie (2005) can be modified and applied to the stress calculation of the reinforcing bar in the cracked section, which was defined as the following **Eq. 22**. In the equations given earlier, the parameters or coefficients can refer to the existing literature (Song et al., 2020). By solving **Eq. 21** and **Eq. 22**, the cycle-dependent stress of the reinforcing bar can be obtained.

FIGURE 3 | Sub-element discretization.

FIGURE 4 | Translational equilibrium of the sub-domain: **(A)** in the left part of a sub-element and **(B)** in the right part of a sub-element.

$$A_r^f(n) = A_r \left[1 - n \big/ N_{f3} \left(1 - \sigma_s(n) \big/ f_{sy} \right) \right] \tag{21}$$

$$\sigma_s(n) = \frac{E_s A_s \left(\varepsilon_{r0}^f I_0^f y_0 - \varepsilon_s^f I_s y_{0r}^f \right)}{\left[\left(A_r^f(n) + A_s \right) I_s + A_r^f(n) A_s y_0^2 \right] y_{0r}^f}. \tag{22}$$

Analytical Formulation of a Sub-Element

The mechanical approach to investigating the crack opening of a cracked beam is based on knowledge of the crack position (stabilized cracking) (Fabbrocino et al., 2007). Due to the randomness and complexity of the cracks' development, the following two assumptions are made to simplify the model problem:

(1) The main crack occurs at the position of maximum bend.
(2) The profiles of cracks are linear triangular.

Each sub-element is defined between two adjacent cracks, that is, on the average crack spacing $l_{c,r}$, as shown in **Figure 3**. The nodes for a sub-element discretization based on the finite difference method are also presented in **Figure 3**, as well as the details of the composite beams. According to a generic approach used in reinforcement concrete beams (Oliveira et al., 2008), the theoretical analysis of a sub-element can be referred to a sub-domain with a length of dx of the concrete slab, as shown in **Figure 4**, where the cases of the shear-slip behavior at the beam–slab interface and bond–slip behavior at the reinforcement–concrete interface are schematically reported

FIGURE 5 | Flowchart of the numerical solution of crack width.
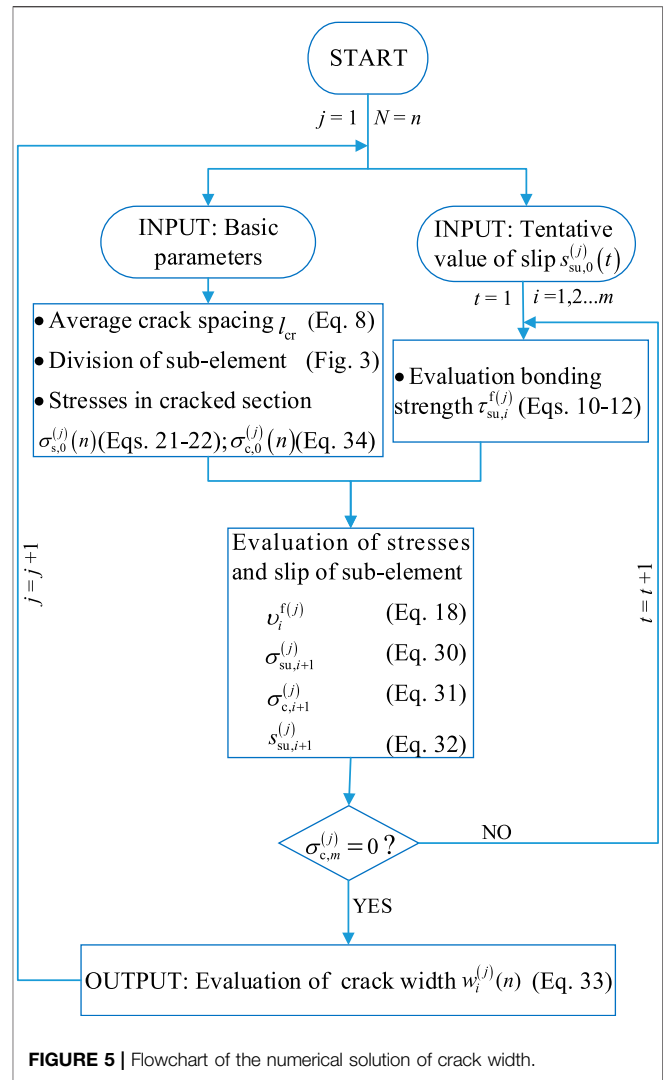
together with some issues related to the boundary conditions. Then the axial force equilibrium of the bar and the cross-section under fatigue loading at a certain number of repeated cycles n can be expressed as follows:

$$d\sigma_u(n) A_u^f = \mp \pi \tau_u^f d_u dx, \tag{23}$$

$$d\sigma_b(n) A_b^f = \mp \pi \tau_b^f d_b dx, \tag{24}$$

$$d\sigma_c(n) A_{eff} = \mp n_u A_u^f d\sigma_u(n) \mp n_b A_b d\sigma_b(n) - v_n dx, \tag{25}$$

where $d\sigma_u(n)$ and $d\sigma_b(n)$ are the stress increments under fatigue loading of reinforcement bars in the top layer and bottom layer, respectively; τ_u^f and τ_b^f are the bonding strengths under fatigue loading of reinforcement bars; d_u and d_b are the diameters of reinforcement bars; n_u and n_b are the numbers of reinforcement bars; $d\sigma_c$ is the stress increments of the tension concrete under fatigue loading; A_{eff} is the effective tension area of the concrete slab; A_u^f and A_b^f are the areas of reinforcement bars under fatigue loading; dx is the length of the sub-domain of the concrete slab; and $\mp$ or $\pm$ depends on the position of the sub-domain.
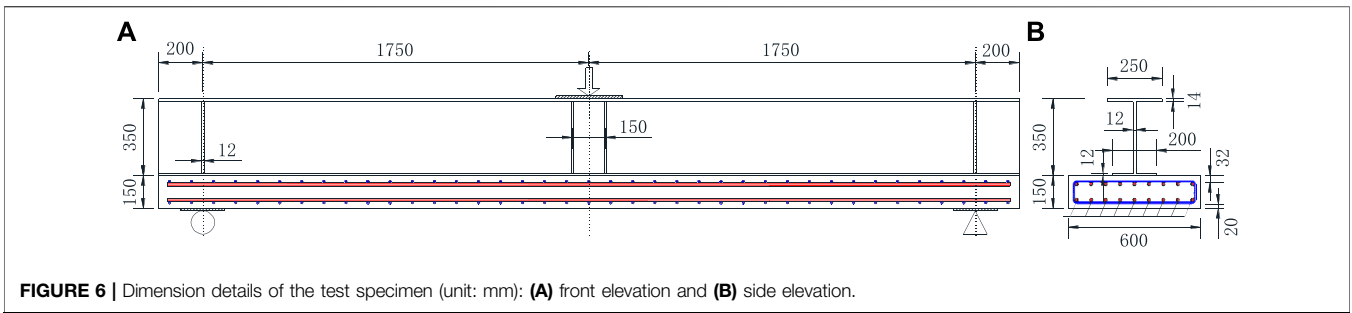
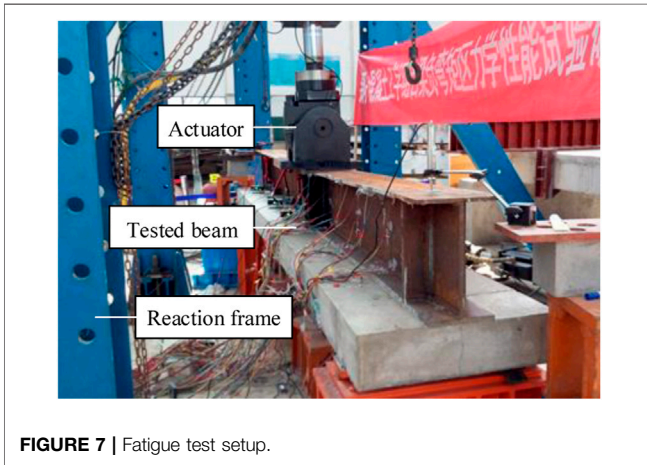**FIGURE 6 |** Dimension details of the test specimen (unit: mm): **(A)** front elevation and **(B)** side elevation.

FIGURE 7 | Fatigue test setup.

According to **Eqs 23**, **24**, the distribution coefficient of the tress increments of reinforcement bars can be defined as follows:

$$\xi = \frac{d\sigma_b(n)}{d\sigma_u(n)} = \frac{\tau_b^f}{\tau_u^f} \frac{d_u}{d_b}. \tag{26}$$

Based on assumption 2, the following equation is obtained:

$$s_u^f = \frac{h_u}{h_b} s_b^f, \tag{27}$$

where s_u^f and s_b^f are the slips of reinforcing bars in the top layer, and bottom layer, respectively; h_u and h_b are the distances of the beam–slab interface to reinforcing bars.

Then the stress increments of the tension concrete can be expressed as follows:

$$d\sigma_c(n) = \frac{\mp n_u A_u^f d\sigma_u(n) \mp n_b \xi A_b d\sigma_u(n) - \nu_n dx}{A_{eff}}. \tag{28}$$

Analytical Model for Crack Width

The stress variable in a sub-element depends on the relative slip between reinforcing bars and surrounding concrete, that is, the difference in longitudinal displacements between them. Thus, this description can be given as follows:

$$\frac{ds(x)}{dx} = \frac{d[u_s(x) - u_c(x)]}{dx} + \varepsilon_{sh} = \varepsilon_s(x) - \varepsilon_c(x) + \varepsilon_{sh}, \tag{29}$$

where $u_s(x)$ and $u_c(x)$ are the longitudinal displacements of reinforcement bars and surrounding concrete, respectively; $\varepsilon_s(x)$ and $\varepsilon_c(x)$ are, respectively, the strains of reinforcement bars and surrounding concrete; ε_{sh} is the shrinkage strain of concrete, and $\varepsilon_{sh} = 310\mu$ is for this work according to China Code GB 50917-2013 (2013).

According to the division for the sub-element with small length Δx (see **Figure 4**), the finite difference forms of <b> **Eqs 23**, **28**, **29** are as follows:

$$\sigma_{su,i+1}^{(j)}(n) = \sigma_{su,i}^{(j)}(n) \mp \frac{4}{d_u} \tau_{su,i}^{f(j)} \Delta x, \tag{30}$$

$$\sigma_{c,i+1}^{(j)}(n) = \sigma_{c,i}^{(j)}(n) + \frac{\pm (n_u d_u + n_b \xi d_b) \pi \tau_{su,i}^{f(j)} - \nu_i^{(j)}}{A_{eff}} \Delta x, \tag{31}$$

$$s_{su,i+1}^{f(j)} = s_{su,i}^{f(j)} \mp \left(\frac{\sigma_{su,i+1}^{(j)}(n) + \sigma_{su,i}^{(j)}(n)}{2E_s} - \frac{\sigma_{c,i+1}^{(j)}(n) + \sigma_{c,i}^{(j)}(n)}{2E_c} + \varepsilon_{sh} \right) \Delta x. \tag{32}$$

The values of σ_{su} and σ_c in the $i+1$ section are determined from the values attained in the i section, by using the method of finite difference (Castel et al., 2012). Based on the bond–slip theory, the crack widths of steel–concrete composite beams under hogging moment can be expressed as follows:

$$w_i^{(j)}(n) = \begin{cases} 2s_{su,0}^{f(j)} & j = 1 \ , \ i = 0 \\ s_{su,0}^{f(j-1)} + s_{su,m}^{f(j)} & j > 1 \ , \ i = 0 \\ 2s_{su,m}^{f(j)} & j = k, \ i = m. \end{cases} \tag{33}$$

The boundary conditions in the cracked section $x=(j-1)l_{cr}$ of each sub-element numbered j applied to **Eqs 31–33** can be expressed as follows:

$$\sigma_{s,0}^{(j)}(n) \neq 0; \ \sigma_{c,0}^{(j)}(n) = 0. \tag{34}$$

And the boundary condition at the abscissa $x = jl_{cr}$ established as the condition of convergence can be given in the following form:

$$\sigma_{c,m}^{(j)}(n) = 0. \tag{35}$$

Figure 5 shows the flowchart of the procedure for numerical solution. Through giving a tentative value $s_{su,0}$, it is possible to

TABLE 3 | Typical experimental results.

Specimen	Load mode	Fatigue load (kN)			F_{cr} (kN)	F_u or F'_u (kN)	Repeated cycles (10^4)	N_f (10^4)	Failure mode
		F_{max}	F_{min}	ΔF					
SCB1-1	Static	—	—	—	70	1,033	—	—	Compression buckling of bottom profile
SCB1-2	Fatigue	250	25	225	68	973	250	—	No fatigue failure
SCB1-3	Fatigue	400	40	360	67	477	152	152	Fatigue cracking of top profile
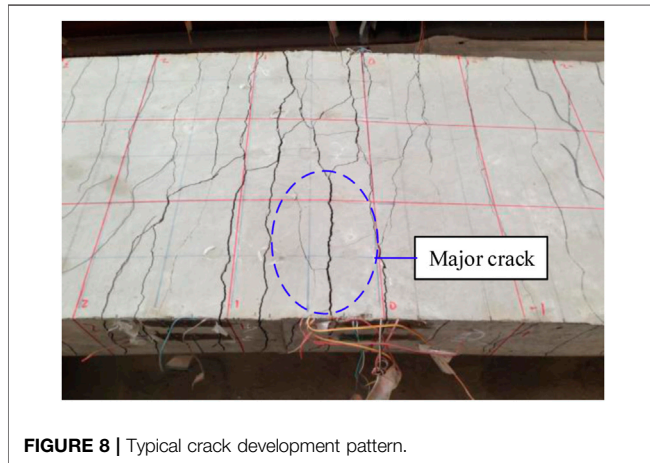
FIGURE 8 | Typical crack development pattern.

predict the crack widths along the composite beam corresponding to a certain loading level. The specific steps are as follows:

1) Input basic information and data of composite beam. Calculate the average crack spacing l_{cr} according to **Eq. 8**. Divide a half-span structure into k sub-elements. Divide a sub-element into m sub-domains. Take the sub-element (i.e., numbered j) as the research object and input the repeated cycles n. Obtain the reinforcement stress $\sigma_{s,0}(n)$ at the cracked section by combining **Eq. 21** and **Eq. 22**. Calculate the concrete stress $\sigma_{c,0}(n) = 0$ at the cracked section by **Eq. 34**.

2) Assume the slip between the reinforcing bar and the concrete at the initial cracked section (i.e., the node number is $i = 0$) as an arbitrary value. Use **Eq. 10** and **Eq. 12** to modify **Eq. 11**, and obtain the bond–slip constitutive relation between the reinforcing bar and concrete under fatigue loading. Calculate the bond stress $\tau_{su,i}^f$ on sub-domain numbered $i+1$. Calculate the shear force v_i^f of unit length at the beam–slab interface on sub-domain numbered $i+1$ by **Eq. 18**.

3) Calculate reinforcing bar stress $\sigma_{su,i+1}(n)$, concrete stress $\sigma_{cu,i+1}(n)$ and the slip $s_{su,i+1}^f$ between reinforcing bar and concrete by **Eqs 30–32**.

4) Set $i = i+1$ and repeat Step 3 until $i = m$, on the condition of the initial set of slip value $s_{su,0}$ and number of iterations of $t = 1$. Calculate the crack width according to **Eq. 33** if the concrete stress $\sigma_{c,m} = 0$ or within the allowable error range, according to the control condition in **Eq. 35**. If $\sigma_{c,m} \neq 0$ or the allowable error is exceeded, correct the initial slip value $s_{su,0}$ and continue the iterative operation of $t = t+1$ (i.e., repeat steps 2–4), until you get a reasonable value.
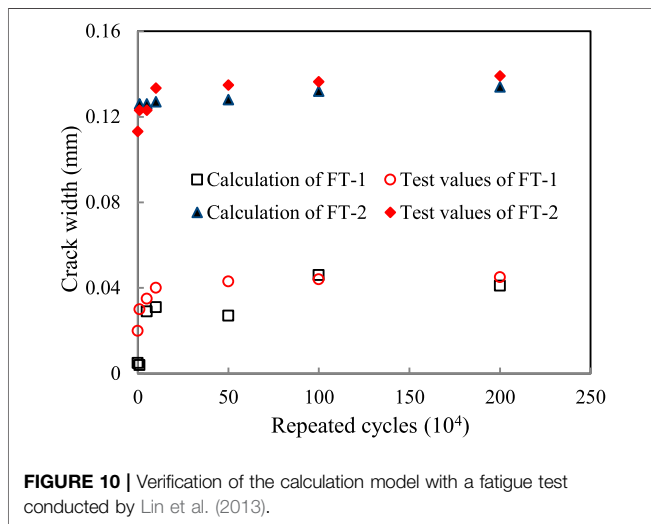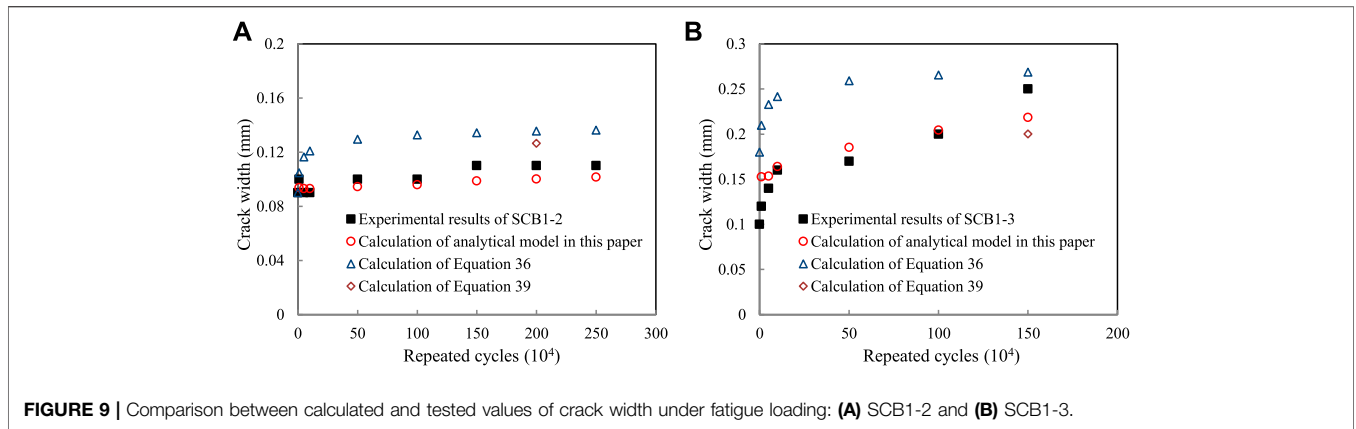
MODEL VALIDATION

Outline of the Experiment

In order to obtain the experimental values of crack width in the negative moment regions of steel–concrete composite beams under fatigue loading, a total of three test beams were designed and manufactured. The specimens were placed upside down on two steel supports to simulate the action of a negative moment. Among them, the specimen numbered SCB1-1 was used for a static loading test, while the specimens numbered SCB1-2 and SCB1-3 were used for fatigue loading tests. **Figure 6** shows the dimension details of the specimens. All test beams are equipped with stud connectors with a diameter, height, and spacing of 16 mm, 90 mm, and 100 mm, respectively. The ratio of longitudinal reinforcing bars is designed as 4.0% with a diameter of 16 mm. Material tests were conducted on concrete and steel before the formal loading of the specimens. The strength grade of the concrete was designed to be C50. The tensile reinforcement bars and steel plates used HRB400 and Q345, respectively (of the same factory batch). The axial tensile strength, elastic modulus, and the average result of compressive strength of concrete are 3.44 MPa, 3.47×10^4 MPa, and 51.2 MPa, respectively. Meanwhile, the average results of the tensile yield strengths of the web (or top flange), bottom flange, and reinforcing bars are 443 MPa, 391 MPa, and 592 MPa, respectively. The setup of the fatigue test is illustrated in **Figure 7**. The fatigue load limits of SCB1-2 and SCB1-3 were designed as 25%F_u and 40%F_u, where F_u is the ultimate bearing capacity of SCB1-1 obtained from the static test. The loading ratio and frequency were set as 0.1 and 2 Hz, respectively. And the sine wave was used for the fatigue loading. The fatigue loading was suspended when the repeated cycles reached the specified times of 1×10^4, 5×10^4, 10×10^4, 50×10^4, 100×10^4, 150×10^4, 200×10^4, and 250×10^4. Then the static loading test was performed to measure the crack width by an electronic crack width measurement instrument. The typical experimental results are listed in **Table 3**, in which ΔF is the fatigue load amplitude, that is, $F_{max} - F_{min}$; F_{cr} is the cracking load in a static test; N_f is the fatigue life. The typical pattern of crack development is shown in **Figure 8**.

Existing Calculation Methods for Crack Width Under Fatigue Loading

The relative slip between the reinforcing bar and concrete increases gradually under the action of fatigue load, resulting in the growth of crack width with repeated cycles. At

FIGURE 9 | Comparison between calculated and tested values of crack width under fatigue loading: **(A)** SCB1-2 and **(B)** SCB1-3.

FIGURE 10 | Verification of the calculation model with a fatigue test conducted by Lin et al. (2013).

present, there is no specific method to calculate the crack width in the negative moment regions of composite beams under fatigue loading. For reinforced concrete structures, the crack width under fatigue loading is generally expressed by the method under static loading through appropriate correction, that is, the experimental regression formula obtained by using the initial crack expansion coefficient (Song, 2006). According to the test results, a statistical empirical formula was given for the maximum crack width after n loading cycles:

$$\omega_{max} = \omega_0 \left(0.382 - 0.0227 \lg n\right) \lg n, \tag{36}$$

where, ω_0 is the initial maximum crack width, which can be calculated according to the conventional method under static loading. In this study, it is calculated according to the recommended formula in JTG D62-2004 (2004), which is expressed as follows:

$$\omega_0 = C_1{'} C_2{'} C_3{'} \frac{\sigma_s}{E_s} \left(\frac{30 + d_{eq}}{0.28 + 10\rho}\right), \tag{37}$$

$$\rho = \frac{A_r + A_p}{bh_0 + (b_f - b)h_f}, \tag{38}$$

where A_p is the area of prestressed reinforcement in the tensile zone; b_f and h_f are the width and thickness of the tensile concrete slab; $C_1{'} = 1.0$ is for the deformed bar; $C_2{'} = 1.0$ is for load effect; $C_3{'} = 1.2$ is for the axial tension members.

In GB 50010-2010 (2010), the non-uniform coefficient φ of tensile rebar strain for reinforced concrete specimens under fatigue loading is equivalent to 1.0, that is, the bond between the rebar and the concrete fails completely, considering the fatigue effect. The calculation method is proposed based on the assumptions that the fatigue failure occurs in reinforced concrete structures or the loading cycles reaches 200×10^4, and the maximum crack width can be expressed as follows:

$$\omega_{max} = \alpha_{cr} \frac{\sigma_s}{E_s} \left(1.9 c_s + 0.08 \frac{d_{eq}}{\rho_{eq}}\right), \tag{39}$$

where α_{cr} is the characteristic coefficient of tension members under the action of force; f_{tk} is the standard value of concrete tensile strength; for other coefficients, refer to the explanation given before.

Verification of the Calculation Model

Figure 9 shows the load–crack width response of the experimental test, the existing calculation methods, and the proposed model in this study. It can be found that the crack width measured in the test increased with the repeated cycles. It developed rapidly in the early loading process of about 10×10^4 cycles, and then grew slowly. The crack width calculated according to **Eq. 36** had a large deviation from the test results at different times of cyclic loading. The results of the maximum crack width by **Eq. 39** were limited to a particular condition. In addition, the calculated values were not universal for the structure checking and were not in good agreement with the test results. As for the numerical model in this study, which fully takes the characteristics of the negative moment regions of composite beams into consideration, the computed results are in good agreement with the experimental values. And the accuracy was further verified by the tested values from other literature (Lin

et al., 2013), as shown in **Figure 10**. As a result, the numerical model can well reflect the development trend of crack width in the process of fatigue loading and provide a reference for anti-fatigue design and checking calculation of composite beam in negative moment region.

CONCLUSION

In this study, a modified formula for average crack spacing and a numerical model for crack width in hogging moment regions of steel–concrete composite beams under fatigue loading are presented. Meanwhile, an experimental test is designed and conducted to obtain the crack width at certain repeated cycles. Then the accuracy of the proposed analytical models is validated through the comparison between the proposed models and test results. The main conclusions drawn are as follows:

(1) The modified formula of average crack spacing takes the spacing of transverse reinforcement into account through the analysis and discussion of existing equations. By comparison, the modified formula shows more reasonable results.

(2) The analytical model for crack width under repeated loading includes the explicit formulations of slip at both the beam–slab interface and the reinforcement–concrete interface, as well as reinforcement stress in the cracked section considering fatigue effect. The analytical results can be obtained by using a suitable numerical procedure.

(3) Compared with the empirical formulas for crack width under fatigue loading based on the axial tension members in existing literature, the analysis results of the numerical

model show more reasonable agreement with the measured values of the experimental beams conducted in this study. For engineering design and application, the work in this study can provide a reference for calculation and evaluation in the negative moment regions of steel–concrete composite beams under fatigue loading.

DATA AVAILABILITY STATEMENT

The original contributions presented in the study are included in the article/Supplementary Material, further inquiries can be directed to the corresponding authors.

AUTHOR CONTRIBUTIONS

AS conceived the work and wrote the manuscript. AS, HX, and QL developed the analytical model. SW analyzed the results and revised the manuscript. All authors read and agreed to the published version of the manuscript.

FUNDING

REFERENCES

Balázs, G. (1991). Fatigue of Bond. *ACI Mater. J.* 88 (6), 620–629.

BS EN 1992 Eurocode 2 (2004). *Design of Composite concrete Structure*. Brussels, Belgium: European Committee for Standardization.

BS EN 1994-2 (2005). *Eurocode 4: Design of Composite Steel and concrete Structures, Part 2: General Rules and Rules for Bridges*. Brussels, Belgium: European Committee for Standardization.

Castel, A., Vidal, T., and François, R. (2012). Finite-element Modeling to Calculate the Overall Stiffness of Cracked Reinforced concrete Beams. *J. Struct. Eng.* 138 (7), 889–898. doi:10.1061/(ASCE)ST.1943-541X.0000520

CEB-FIP Model Code 1978 (1978). *CEB-FIP Model Code 1978*. Lausanne, Switzerland: Comite Euro-International du Beton, Thomas Telford Ltd.

CEB-FIP Model Code 1990 (1993). *CEB-FIP Model Code 1990*. Lausanne, Switzerland: Comite Euro-International du Beton, Thomas Telford Ltd.

Chen, S., Wang, X., and Jia, Y. (2009). A Comparative Study of Continuous Steel-concrete Composite Beams Prestressed with External Tendons: Experimental Investigation. *J. Constructional Steel Res.* 65 (7), 1480–1489. doi:10.1016/j.jcsr.2009.03.005

El-Shihy, A. M., Fawzy, H. M., Mustafa, S. A., and El-Zohairy, A. A. (2010). Experimental and Numerical Analysis of Composite Beams Strengthened by CFRP Laminates in Hogging Moment Region. *Steel Compos. Structures* 10 (3), 281–295. doi:10.12989/scs.2010.10.3.281

El-Zohairy, A., Salim, H., Shaaban, H., Mustafa, S., and El-Shihy, A. (2017). Experimental and FE Parametric Study on Continuous Steel-concrete Composite Beams Strengthened with CFRP Laminates. *Construction Building Mater.* 157, 885–898. doi:10.1016/j.conbuildmat.2017.09.148

Fabbrocino, G., Verderame, G. M., and Polese, M. (2007). Probabilistic Steel Stress-Crack Width Relationship in R.C. Frames with Smooth Rebars. *Eng. Structures* 29 (1), 1–10. doi:10.1016/j.engstruct.2006.04.002

Fan, J., Gou, S., Ding, R., Zhang, J., and Shi, Z. (2020). Experimental and Analytical Research on the Flexural Behaviour of Steel-ECC Composite Beams under Negative Bending Moments. *Eng. Structures* 210 (1), 110309.1–110309.17. doi:10.1016/j.engstruct.2020.110309

Fan, J., and Nie, J. (2005). Effects of Slips on Load-Carrying Capacity of Composite Beams under Negative Bending. *Eng. Mech.* 22 (3), 177–182. doi:10.3969/j.issn.1000-4750.2005.03.031

GB 50010-2010 (2010). *Code for Design of concrete Structures*. Beijing, China: Ministry of Construction of China.

GB 50917-2013 (2013). *Code for Design of Steel and concrete Composite Bridges*. Beijing, China: Ministry of Construction of China.

GBJ 10-89 (1989). *Code for Design of concrete Structures*. Beijing, China: Ministry of Construction of China.

Han, J., Song, Y., and Chang, J. (2014). Analysis Model of Crack Width of Partially Prestressed concrete Beams under Fatigue Loading. *J. Cent. South Univ. (Science Technology)* 45 (11), 3977–3985. JournalArticle/5b433a76c095d716a4bf90c3.

Hanswille, G., Porsch, M., and Ustundag, C. (2007a). Resistance of Headed Studs Subjected to Fatigue Loading. *J. Constructional Steel Res.* 63 (4), 475–484. doi:10.1016/j.jcsr.2006.06.035

Hanswille, G., Porsch, M., and Ustundag, C. (2007b). Resistance of Headed Studs Subjected to Fatigue Loading Part II: Analytical Study. *J. Constructional Steel Res.* 63 (4), 485–493. doi:10.1016/j.jcsr.2006.06.036

He, J., Liu, Y., Chen, A., and Yoda, T. (2010). Experimental Study on Inelastic Mechanical Behaviour of Composite Girders under Hogging Moment. *J. Constructional Steel Res.* 66 (1), 37–52. doi:10.1016/j.jcsr.2009.07.005

Hou, W., Luo, R., and Ye, M. (2001). On Crack Width of Steel Cast-In-Place concrete Composite Beams with High Reinforcement Ratio. *China Railway Sci.* 22 (5), 54–60. doi:10.3321/j.issn:1001-4632.2001.05.009

JTG D62-2004 (2004). *Code for Design of Highway Reinforced concrete and Prestressed concrete Bridges and Culverts*. Beijing, China: Ministry of Communication of China.

Lin, W., Yoda, T., and Taniguchi, N. (2013). Fatigue Tests on Straight Steel-concrete Composite Beams Subjected to Hogging Moment. *J. Constructional Steel Res.* 80 (1), 42–56. doi:10.1016/j.jcsr.2012.09.009

Liu, F., and Zhou, J. (2018). Experimental Research on Fatigue Damage of Reinforced Concrete Rectangular Beam. *KSCE J. Civ. Eng.* 22 (9), 3512–3523. doi:10.1007/s12205-018-1767-y

Liu, J., Ding, F.-x., Liu, X.-m., and Yu, Z.-w. (2016). Study on Flexural Capacity of Simply Supported Steel-concrete Composite Beam. *Steel Compos. Struct.* 21 (4), 829–847. doi:10.12989/scs.2016.21.4.829

Luo, Q., Liu, D., Qiao, P., Zhou, Z., Zhao, Y., and Sun, L. (2020). Micro-CT-based Micromechanics and Numerical Homogenization for Effective Elastic Property of Ultra-high Performance concrete. *Int. J. Damage Mech.* 29 (1), 45–66. doi:10.1177/1056789519848475

Manfredi, G., Fabbrocino, G., and Cosenza, E. (1999). Modeling of Steel-concrete Composite Beams under Negative Bending. *J. Eng. Mech.* 125 (6), 654–662. doi:10.1061/(asce)0733-9399(1999)125:6(654)

Manfredi, G., and Pecce, M. (1998). A Refined R.C. Beam Element Including Bond-Slip Relationship for the Analysis of Continuous Beams. *Comput. Structures* 69 (1), 53–62. doi:10.1016/S0045-7949(98)00078-9

Nie, J., and Zhang, M. (1997). Study on the Crack of concrete Flange in Tension of Composite Steel-concrete Beams. *J. Tsinghua Univ. Sci. Technol.* 37 (6), 95–99. doi:10.3321/j.issn:1000-0054.1997.06.004

Oliveira, R. S., Ramalho, M. A., and Corrêa, M. R. S. (2008). A Layered Finite Element for Reinforced concrete Beams with Bond-Slip Effects. *Cement and Concrete Composites* 30 (3), 245–252. doi:10.1016/j.cemconcomp.2007.09.007

Qin, F., Zhang, Z., Yin, Z., Di, J., Xu, L., and Xu, X. (2020). Use of High Strength, High Ductility Engineered Cementitious Composites (ECC) to Enhance the Flexural Performance of Reinforced concrete Beams. *J. Building Eng.* 32, 101746. doi:10.1016/j.jobe.2020.101746

Ramm, W., and Elz, S. (2002). "Composite Construction in Steel and Concrete IV," in Proceedings of Composite Construction in Steel and Concrete IV Conference (Fairfax, America: ASCE Press). doi:10.1061/9780784406168

Ryu, H.-K., Chang, S.-P., Kim, Y.-J., and Kim, B.-S. (2005). Crack Control of a Steel and concrete Composite Plate Girder with Prefabricated Slabs under Hogging Moments. *Eng. Structures* 27 (11), 1613–1624. doi:10.1016/j.engstruct.2005.05.015

Ryu, H.-K., Kim, Y.-J., and Chang, S.-P. (2007). Crack Control of a Continuous Composite Two-Girder Bridge with Prefabricated Slabs under Static and Fatigue Loads. *Eng. Structures* 29 (6), 851–864. doi:10.1016/j.engstruct.2006.06.021

Ryu, H.-K., Shim, C.-S., Chang, S.-P., and Chung, C.-H. (2004). Inelastic Behaviour of Externally Prestressed Continuous Composite Box-Girder Bridge with Prefabricated Slabs. *J. Constructional Steel Res.* 60 (7), 989–1005. doi:10.1016/j.jcsr.2003.09.004

Song, A., Li, Z., Xu, H., Wan, S., and Zhou, P. (2021). Numerical Calculation Model of Crack Width in Negative Moment Regions of Steel-concrete Composite Beams. *J. Harbin Inst. Technol.* 53 (3), 75–81. doi:10.11918/201912134

Song, A., Luo, Q., Wan, S., and Li, Z. (2020). Experimental and Analytical Study on Deformation Behavior in Hogging Moment Regions of Composite Beams. *Adv. Civil Eng.* 2020 (3), 1–10. doi:10.1155/2020/6630742

Song, Y. P. (2006). *Fatigue Behavior and Design Principle of Concrete Structures*. Beijing, China: China Machine Press.

Su, Q.-T., Yang, G.-T., and Wu, C. (2012). Experimental Investigation on Inelastic Behavior of Composite Box Girder under Negative Moment. *Int. J. Steel Struct.* 12 (1), 71–84. doi:10.1007/s13296-012-1007-0

Sun, Q., Yang, Y., Fan, J., Zhang, Y., and Bai, Y. (2014). Effect of Longitudinal Reinforcement and Prestressing on Stiffness of Composite Beams under Hogging Moments. *J. Constructional Steel Res.* 100 (13), 1–11. doi:10.1016/j.jcsr.2014.04.017

Wang, B., Huang, Q., Liu, X., and Li, W. (2018). Experimental Investigation of Steel-Concrete Composite Beams with Different Degrees of Shear Connection under Monotonic and Fatigue Loads. *Adv. Struct. Eng.* 21 (2), 227–240. doi:10.1177/1369433217717121

Wang, W., Zhang, X.-d., Zhou, X.-l., Wu, L., and Zhu, H.-j. (2021). Study on Shear Behavior of Multi-Bolt Connectors for Prefabricated Steel-concrete Composite Beams. *Front. Mater.* 8, 625425. doi:10.3389/fmats.2021.625425

Wu, Z., Chen, H., Gao, X., and Zhu, P. (1993). Experimental Study on Crack Width of concrete Slab of Composite Beams under Negative Bending. *J. Harbin Architecture Civil Eng. Inst.* 26 (1), 58–62.

Yu, Z., and Guo, F. (2004). Experimental Study of Crack Width in Negative Bending Region of Partially Prestressed Continuous Steel concrete Composite Beams. *J. Building Structures* 25 (4), 55–59. doi:10.3321/j.issn:1000-6869.2004.04.008

Zanuy, C., Albajar, L., and de la Fuente, P. (2010). On the Cracking Behaviour of the Reinforced concrete Tension Chord under Repeated Loading. *Mater. Struct.* 43 (5), 611–632. doi:10.1617/s11527-009-9516-9

Zhang, W., Ye, Z., Gu, X., and Li, S. (2017). Assessment of Fatigue Life for Corroded Reinforced concrete Beams under Uniaxial Bending. *J. Struct. Eng.* 143 (7), 04017048 1–14. doi:10.1061/(asce)st.1943-541x.0001778

Zhang, Y., Fan, J., and Li, Y. (2011). Law of Crack Development and Calculation of Crack Width of Continuous Composite Beams. *Eng. Mech.* 28 (7), 84–90. doi:10.1080/0144929X.2011.553739

Zhang, Z., Liu, D., Ding, Y., and Wang, S. (2022). Mechanical Performance of Strain-Hardening Cementitious Composites (SHCC) with Bacterial Addition. *J. Infrastruct. Preserv. Resil.* 3 (3). doi:10.1186/s43065-022-00048-3

Zhang, Z., Liu, S., Yang, F., Weng, Y., and Qian, S. (2021). Sustainable High Strength, High Ductility Engineered Cementitious Composites (ECC) with Substitution of Cement by rice Husk Ash. *J. Clean. Prod.* 317, 128379. doi:10.1016/j.jclepro.2021.128379